ELSEVIER

Journal of Chromatography A, 925 (2001) 171–182

JOURNAL OF CHROMATOGRAPHY A

www.elsevier.com/locate/chroma

# Retention behaviour of amylopectins in asymmetrical flow field-flow fractionation studied by multi-angle light scattering detection

M. van Bruijnsvoort,[a,b], K.-G. Wahlund[a,*], G. Nilsson[c], W.Th. Kok[b]

[a]*Division of Technical Analytical Chemistry, Centre for Chemistry and Chemical Engineering, Lund University, P.O.B. 124, S-22100 Lund, Sweden*

[b]*Department for Chemical Engineering, Polymer-Analysis Group, University of Amsterdam, Nieuwe Achtergracht 166, 1018 WV Amsterdam, The Netherlands*

[c]*Division of Analytical Chemistry, Centre for Chemistry and Chemical Engineering, Lund University, P.O.B. 124, S-22100 Lund, Sweden*

Received 19 March 2001; received in revised form 6 June 2001; accepted 7 June 2001

**Abstract**

Asymmetrical flow field-flow fractionation (FFF) with multi-angle light scattering (MALS) detection was applied for the fractionation of amylopectins from four different sources. Samples originated from genetically modified potatoes and waxy maize. Amylopectins were dissolved in a 1 mol $l^{-1}$ sodium hydroxide solution or water. With an injected mass of 0.2 μg, well below overloading conditions, a decrease of the apparent hydrodynamic radius with increasing inlet flow-rate was observed. Moreover, a decrease of the radius of gyration with increasing elution volume was recorded by the MALS detector. Steric/hyperlayer effects are a feasible explanation for this behaviour. The observed radius of gyration at the steric inversion point was in the order of 0.3 μm, which is smaller than the theoretically calculated inversion point. Apparently, the amylopectin behave as macromolecules with a larger hydrodynamic radius than expected on basis of their radius of gyration and are subjected to significant lift forces. The results were confirmed by four fractionations with varying flow-rates but constant ratio of cross to outlet-flow. In contrast to the normal mode operation, the retention of the amylopectins depended strongly on the applied flow-rates and was close to that of a much smaller 10 kDa dextran. Apparent molar masses in the order of between $10^7$ and $10^9$ g $mol^{-1}$ were obtained. The results are contrasted with enzymatically degraded and oxidised starch samples that were fractionated in the normal mode. 

*Keywords:* Flow field-flow fractionation; Multi angle light scattering detection; Amylopectins

## 1. Introduction

The use of starches and their derivatives is widespread in numerous branches of, e.g., food, paper, adhesive, textile and cosmetic industries [1]. The main constituent of starch is poly-glycopyranose. Two forms of this polysaccharide can be distinguished: amylose, which is slightly branched, and amylopectin, that has a highly branched structure. The industrial importance of starches and related compounds makes an analysis method for their molecular size and molar mass distribution, on which many physical properties depend, desirable.

*Corresponding author. Tel.: +46-46-222-8316; fax: +46-46-222-4525.

*E-mail address:* karl-gustav.wahlund@teknlk.lth.se (K.-G. Wahlund).

0021-9673/01/$ – see front matter 
PII: S0021-9673(01)01020-2

To this purpose, several analytical separation techniques have been applied for the fractionation of amylopectins. These include size-exclusion chromatography (SEC), field-flow fractionation (FFF), capillary electrophoresis [2] and hydrodynamic chromatography in a packed column [3]. The on-line coupling of SEC and FFF with multi-angle light scattering (MALS) detection has grown to be a popular and powerful combination for macromolecular analysis [4]. After the separation technique fractionates the sample according to hydrodynamic radius, MALS provides information concerning the radius of gyration and molar mass of macromolecules. Ideally, the conformation and molar mass distribution of a sample can be obtained from a single measurement.

The application of SEC, the most widely used size analysis method for macromolecules, to the analysis of starches has been reviewed [5]. More recently, various examples of the analysis of amylopectins with SEC–MALS have been reported [6–11]. While SEC is a well-established method for the analysis of degraded starches, the extremely high molar mass of native starches (light scattering experiments have shown that amylopectins have a molar mass of more than $100\times10^6$ g/mole [12]) poses problems for the analysis of these compounds. A low recovery, in the order of 60–80% [6], was observed due to interaction of the starches with the packing material of the column and shear stress degradation cannot be ruled out [7]. Hence, the use of open channels for the separation is potentially advantageous, evading much of the drawbacks connected to a packed column.

Arguably, the most suited group of techniques is field-flow fractionation [13]. Thermal FFF [14] and sedimentation (Sd) FFF [15,16] have already been applied for the analysis of amylopectins. In particular the SdFFF experiments gave an impressive fractionation of high molar mass compounds up to several hundred MDa. However, SdFFF has the disadvantage of a lowest size limit of ca. 50 nm, and of the necessity of a priori knowledge about the density of the analyte to calculate hydrodynamic radii.

It is one of the attractive points of flow FFF that it fractionates samples on basis of their size only, and that it can cover a wide size range within a single run. Since the first coupling of flow FFF with MALS by Roessner and Kulicke [17], it has been employed in numerous analyses, such as of: particles [18], vesicles [19], polysaccharides [20], modified celluloses [21], κ-carrageenan [22,23], xanthan [23], gum arabic [24] and several other food polymers [25].

Of particular interest in this area is a previous study by Wittgren et al., who found for κ-carrageenan indications of a reversal of elution order of large aggregates [22]. They attributed this to ''steric/hyperlayer'' effects. As opposed to the ''normal mode'' FFF, where the retention of the analyte increases with its size, in the steric/hyperlayer mode the retention decreases with the size, since the polymers become sterically hindered to perform their normal Brownian motion [26]. The radius of gyration of amylopectins can be up to 800 nm, which is near the border of the steric regime.

In this study the retention behaviour of amylopectins originating from four different sources is investigated, by combining both retention data from flow FFF and radius data obtained by MALS. Possible mechanisms explaining the behaviour are discussed. For comparison with the amylopectins, two starch samples of relatively low molar mass were fractionated. One was a starch degraded by enzymes and the other an oxidised starch sample. Among the amylopectin samples were amylopectins obtained from genetically modified potatoes, modified in such a way that they only produce trace amounts of amylose.

## 2. Experimental

### 2.1. Instrumental set-up

In Fig. 1 a scheme is presented of the instrumental set-up. This was almost identical to that employed previously [20]. It was used in two different variants, set-ups I and II. In set-up I the detector was a multi-angle light scattering (MALS) detector combined with a differential refractive index (RI) detector. In set-up II the detector was an evaporative light scattering detector. The channels were cut out of a Mylar spacer with a thickness of 130 μm. The channel shape was trapezoidal with length $L=28.6$ cm, and breadths, $b_0$ and $b_1$, 2.1 and 0.54 cm, respectively. In set-up I the accumulation wall was a

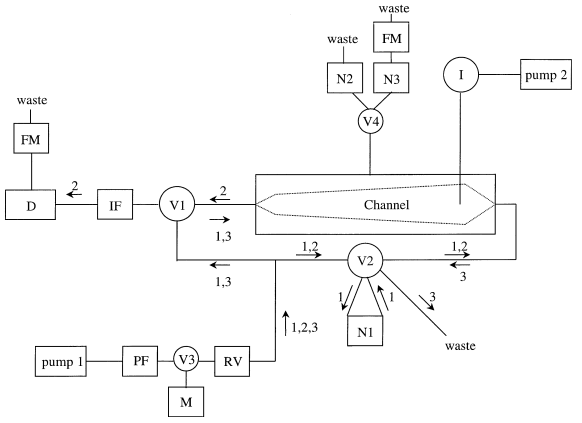


Fig. 1. Scheme of the asymmetrical flow FFF-MALS-RI (set-up I). Legend: **PF** prefilter; **M** Manometer; **RV** Pressure relief valve; **IF** Inline filter (optional); **N** Needle valve; **V** Valve; **I** Injection valve; **FM** Flow meter; **D** Detector(s). The arrows 1, 2 and 3 denote the direction of flow during focusing/relaxation, elution and backflushing of the channel, respectively.

polyaramide membrane UF-PA-20 H (Hoechst, Wiesbaden, Germany) with a molecular mass cut-off of 20 000. This was chosen because initial experiments carried out with a regenerated cellulose membrane gave problems with the baseline of the RI detector, which was thought to be due to poor resistance of the membrane to the high pH of the carrier liquid. In the channel of system II the accumulation wall consisted of a regenerated cellulose ultrafiltration membrane NADIR UF C-10 (Hoechst) having a molecular mass cut-off of 10 000.

Two model 420 liquid chromatography pumps (Kontron Instruments, Zurich, Switzerland) were connected to the channel. Pump 1 delivered the carrier flow and pump 2 was used for the injection. Valves 1 and 2 were a model E-CST 4UV 4 position and EC4 W 2 position motor driven valve, respectively (Vici AG, Valco Europe, Schenkon, Switzerland). Valves 3 and 4 were manually controlled SRV-4 2 port valves (Pharmacia, Uppsala, Sweden). Samples were injected through a 20 μl loop on a 9125 syringe injector (Rheodyne, Cotati, CA, USA). In set-up I a 25 nm cellulose nitrate/acetate prefilter (Millipore Corp., Bedford, MA, USA) with a diameter of 25 mm was installed directly after pump 1. An optional 0.45 μm inline filter of regenerated cellulose (Sartorius AG, Göttingen, Germany) was included between the channel I and the detectors [20]. The upper glass plate of the channel was protected from excessive pressures by a pressure relieve valve (Nupro Co., OH, USA) set at 15 bar. Two needle valves (Hoke, Cresskill, NJ, USA) controlled the cross flow and position of the relaxation point. In set-up I the outlet and cross flow-rate were monitored by flow meters (Phase Separations, Queensferry, UK). In set-up II only the cross flow was monitored.

The evaporative light scattering detector was a DDL 21 (Eurosep Instruments, Cergy-Pontoise, France). The MALS detector was a DAWN-DSP light scattering photometer (Wyatt Technology, Santa Barbara, CA, USA) and the RI detector an Optilab DSP interferometric refractometer photometer (Wyatt Technology), both operating at 633 nm. The RI detector was equipped with a cell with an optical wavelength of 1 mm. Using ASTRA 4.20 software (Wyatt Technology), data were transferred to a personal computer and calculations were performed.

### *2.2. Chemicals and solutions*

All standard chemicals were obtained from the commercial suppliers and were of analytical reagent grade quality. A list of the calibration standards, enzymatically-degraded and oxidised starches, amylopectins and their respective sources is provided in Table 1. The potato amylopectin starches from AVEBE and Lyckeby Stärkelsen were from genetically modified potato. The Lyckeby Stärkelsen sample was specified as amylose deficient (containing less than 2% of amylose). The starches from Sigma and National Starch, originating from waxy corn starch, were received in granular form. The Sigma waxy corn starch is specified as essentially pure amylopectin containing only trace amounts of amylose. In the text, the starch samples are simply termed ‘‘amylopectin’’ and named after their suppliers.

The Lyckeby Stärkelsen and AVEBE potato amylopectin starch were received in easily soluble form, which means that the original granular starch had been pre-gelatinised (the granules were disintegrated/dissolved), precipitated and dried before the dissolution to make the actual samples for the present study. Pre-gelatinisation of the Lyckeby

Table 1
List of standards and amylopectin samples and their suppliers

| Sample | Supplier |
|---|---|
| 0.02 μm PET/carboxylic acid group particles | Bangs Lab., Fishers, IN, USA |
| Ferritin from horse spleen | Sigma, St. Louis, MO, USA |
| Pullulan P-1600 | Showa Denko, Tokio, Japan |
| Enzymatically degraded starch | AVEBE, Groningen, The Netherlands |
| Oxidised starch | AVEBE, Groningen, The Netherlands |
| Starch from potato genetically modified to produce only amylopectin | Lyckeby Stärkelsen, Kristianstad, Sweden |
| Idem | AVEBE, Groningen, The Netherlands |
| Waxy corn starch, unmodified | Sigma, St. Louis, MO, USA |
| Amioca (waxy corn starch) | National Starch and Chemicals Company, Bridgewater, NJ, USA |

Stärkelsen starch had been performed in 90% aqueous DMSO for 72 h during stirring at room temperature. Then the starch was precipitated during 24 h by having first added cold ethanol and then stirred for 24 h at 4°C. The precipitate had been washed, in sequence, with ethanol, acetone, and diethyl ether and thereafter dried in an exsiccator under vacuum. The AVEBE potato amylopectin starch had been pre-treated to disrupt the granules by heating a starch suspension to 165°C during approximately 3 s under high pressure.

Solutions were prepared in demineralised water, that was subsequently deionized through a Milli-Q water purification system (Millipore, Bedford, MA, USA) and filtered through a 0.45 μm filter and a 0.2 μm filter (Sartorius). For set-up I the carrier liquid was an aqueous solution with 5 mmol $l^{-1}$ sodium hydroxide, 0.1 mol $l^{-1}$ sodium chloride and 0.02% (m/v) sodium azide. For set-up I stock solutions of amylopectins, with a concentration of 20 mg $ml^{-1}$, were prepared by 2 h of gentle stirring in a 1 mol $l^{-1}$ sodium hydroxide solution. Fresh solutions were prepared daily. Stock solutions of the enzymatically-degraded and oxidised starches were prepared in a concentration of 100 mg $ml^{-1}$ in a 0.5 mol $l^{-1}$ sodium hydroxide solution.

For set-up II the carrier liquid was de-ionised and filtered water. Fresh solutions of the Lyckeby Stärkelsen amylopectin were prepared daily by dispersing a concentration of 0.75 mg $ml^{-1}$ of pre-gelatinised material in water under gentle stirring. The dispersion was then kept at 85°C for 30 min and subsequently at 120°C for 20 min, under gentle stirring. Before injection these samples were filtered through 5 or 0.45 μm filters and held at 50°C to avoid retrogradation.

### 2.3. Procedures

Detailed descriptions of the operation procedure have been given previously [20,27,28]. The sample was injected during 20 s with an injection flow-rate of 0.2 ml $min^{-1}$. It was focussed for a total of 1.2 min with a flow-rate of 1 ml $min^{-1}$.

During focusing, the cross flow was directed through needle valve N3 to regulate the pressure that was set at a value of 0.2 bar higher than the pressure during the elution mode. This was in order to reduce the pressure difference between focusing/relaxation and elution mode. After relaxation, the system was switched to the elution mode, and valve V3 was turned, so that the cross flow passed through needle valve N2, which regulated the cross flow during elution. An immediate pressure drop of 0.5 bar was observed and in 0.5 min the pressure reached its final value.

The thickness of the channel in set-up I was determined to be 90 μm and that in set-up II 125 μm by triplicate measurements of the elution time of ferritin [28]. The MALS detector was calibrated with filtered toluene and normalised with 0.02 μm PET/carboxylic acid group particles. The determined hydrodynamic radius, r.m.s. radius and molar mass of a 1.6 MDa pullulan standard were all in accordance with values reported previously [20].

For the amylopectins, a dn/dc value of 0.15 ml

$g^{-1}$ [12] was used for the calculations of molar mass. Experiments were performed in duplo.

## 3. Theory

### 3.1. Flow field-flow fractionation

The principles and theory of asymmetrical flow FFF have been described in detail previously [27–30] as well as its application to the size fractionation of water-soluble polymers [20–22]. Samples are retained at different levels according to their average displacement by a perpendicular flow-field in a laminar flow. The dimensionless retention parameter $\lambda$ is in a first approximation related to the retention ratio $R$ (ratio of the void time and the retention time), by:

$$R = 6\lambda\left(\coth\left(\frac{1}{2\lambda}\right) - 2\lambda\right). \quad (1)$$

If the retention is sufficiently high ($R<0.48$) Eq. (1) can be approximated within 10% by $R=6\lambda$ [30]. Then, from the retention parameter the diffusion coefficient can be obtained as:

$$D = \frac{\lambda F_{cr} w}{A} \quad (2)$$

where $F_{cr}$ is the flow-rate of the cross-flow field, w the channel thickness and A the accumulation wall area. Combination of Eq. (2) with the well-known Stokes–Einstein relation enables the hydrodynamic radius $r_H$ to be calculated from the retention time as:

$$r_H = \frac{kTAt_r}{\pi\eta t_0 F_{cr} w} \quad (3)$$

where $\eta$ is the viscosity of the solvent, $k$ the Boltzmann constant, T the temperature and $t_0$ and $t_r$ the void time and retention time, respectively. The void time can be calculated for known inlet flow-rate ($F_{in}$), outlet flow-rate ($F_{out}$), channel dimensions and focusing point position [27].

The above description is valid for flow FFF carried out in the so-called normal mode based on the presence of an exponential concentration distribution of the analyte near the accumulation wall. A steric mode is prevailing when there is a steric exclusion from the accumulation wall, which can be observed for macromolecules or particles larger than ca. 1 μm [31]. This causes a reversal of the elution order. Under many practical conditions this mode is accompanied by a flow-rate-dependent hydrodynamic lift-force, creating so-called hyperlayers. Thus, the hyperlayer mode (a.k.a. lift mode or focusing mode [32]) also leads to a reversal of the elution order [33]. The combined retention mechanism has been termed steric/hyperlayer mode.

### 3.2. Multi-angle light scattering and data analysis

The theory and principle of MALS is well described in the literature [4]. The eluate from the flow FFF instrument is measured in narrow time increments, slice by slice, by the MALS and RI detector. In each slice the MALS instrument measures the excess Rayleigh scattering $R_\theta$ at 16 different angles from 14° to 163°. The molar mass $M$ is related to the excess Rayleigh scattering by the Rayleigh or Rayleigh–Gans–Debye approximation:

$$\frac{R_\theta}{Kc} = MP(\theta)(1 - 2A_2 cMP(\theta)) \quad (4)$$

where $K$ is an instrumental coefficient depending among other things on the refractive index increment of the sample and the wavelength of the incident light, $c$ is the sample concentration (measured by the RI detector in each slice), $A_2$ is the second virial coefficient, and $\theta$ is the scattering angle. $P(\theta)$ is a so-called form factor that depends on the root mean square radius (r.m.s. radius), the latter often termed the radius of gyration, $r_g$, as:

$$P(\theta)^{-1} = 1 + \frac{16\pi^2 < r_g^2 >}{3\lambda^2}\sin^2\left(\frac{\theta}{2}\right) \quad (5)$$

where $\lambda$ is the wavelength of the incident light. This is an approximation in which higher order terms in $\sin^2(\theta/2)$ have been omitted.

The MALS data are evaluated through a Debye plot, depicting a function of the excess Rayleigh scattering against $\sin^2(\theta/2)$. $M$ and $r_g$ are obtained from the intercept and slope, respectively, of the Debye plot extrapolated to 0°, which means that they have to be derived preferably from the observed light scattering at the lowest available angles. To help in the extrapolation in case of a curvature, the ASTRA

software can be used to fit an empirical polynomial to the data points. Alternatively, and especially for macromolecules with a large r.m.s. radius, the extrapolation can be facilitated by not using the data points from the high angles if they present a strong deviation from the slope of the low angle data. Without a concentration detector, only the r.m.s. radius can be determined.

Results from relatively small macromolecules (the two degraded starches in this study) were obtained through a Debye plot performed by the so-called Debye method ($R_\theta/Kc$ vs. $\sin^2(\theta/2)$) giving a linear relationship. The 14° and 26° angles were omitted because they deviated strongly from the linearity of all other angles. The Debye plot for the amylopectins was expressed by the Berry method ($(Kc/R_\theta)^{1/2}$ vs. $\sin^2(\theta/2)$) using a 2nd order polynomial fit to take care of a curvature at the low angles [12]. Only the data from seven angles of between 14° to 90° were used because the angles above those gave a deviating slope that approached zero.

There are various contributions to errors in the results obtained by MALS analysis, that may lead to significant deviations from the true values when very large molecules are analysed. Since the density of amylopectins is typically smaller than that of compact particles only a small contribution of Mie scattering is to be expected [12]. However, there is the effect of $A_2$ that has not been taken into account in this work. For example, the introduction of a typical $A_2$ value of $2\times10^{-5}$ mol ml $g^{-2}$ for a 100 MDa polymer can lead to a difference of up to 30% in calculating the molar mass value [34]. For large macromolecules there is the possibility that the Rayleigh approximation no longer holds. In addition, the extrapolation of the non-linear curve in the Berry method from 14° to 0° introduces an uncertainty. Therefore, the molar masses determined in the present study will have to be regarded as only approximate. Moreover, they should be regarded as apparent molar masses because the macromolecules may be partly present in aggregated form.

## 4. Results and discussion

### 4.1. Degraded starch samples

For comparison with the amylopectins, two samples of degraded starches were fractionated. Fig. 2A shows a fractogram of an enzymatically-degraded starch while Fig. 2B shows a fractogram of an oxidised starch. In order to improve the signal-to-noise-ratio of the MALS detector for the lower angles, the fractogram of the enzymatically-degraded

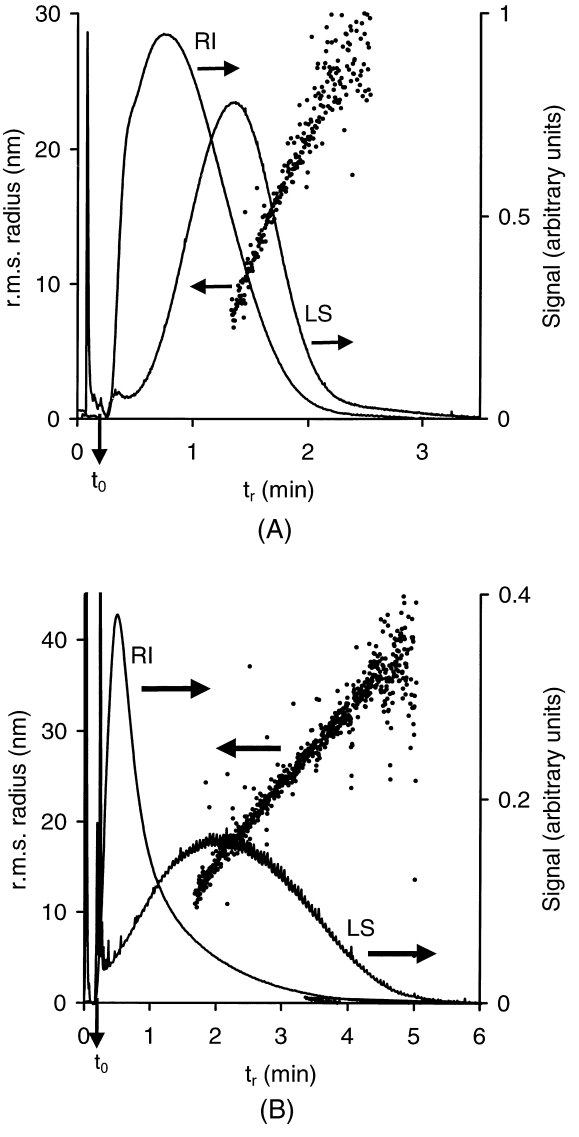


Fig. 2. A (upper): RI and 90° LS fractogram of an enzymatically degraded starch sample with obtained r.m.s. radii. Set-up I. The calculated $t_0$ is indicated. $F_{in}$:$F_{cr}$ = 3.0:2.2 ml $min^{-1}$; injected mass: 200 μg. B (lower): RI and 90° LS fractogram of an oxidised starch with obtained r.m.s. radii. Set-up I. The calculated $t_0$ is indicated. $F_{in}$:$F_{cr}$ = 2.0:0.70 ml $min^{-1}$; injected mass: 100 μg.

starch was obtained with a 0.45 μm in-line filter placed between the FFF channel and the detectors. Both fractograms show the opportunity of rapid fractionation and the suitability and limitations of the flow FFF-MALS combination for the characterisation of starches of relatively low molar mass [35]. It is possible that a fraction of the low-molar mass end of the distribution (less than 20 kDa) may have been lost through the membrane. Moreover, the r.m.s. radius of a substantial amount of material is in the range of smaller than 10 nm, which is the lower size detection limit of the MALS detector, and therefore not measurable. At the high size end the accuracy in the determination of the molar mass decreases when the detection limit for the RI signal is reached. Thus the r.m.s. radius and molar mass can only be obtained for a limited size range. It can be seen that the enzymatic treatment was more efficient than the oxidation in degrading the starch since the oxidised product contains larger molecules.

Note that in Fig. 2B the r.m.s. radius increases linearly with the retention time between 2 and 4 min and that, from this range, the extrapolated intercept is close to zero. Assuming a uniform conformation of the starches (so that there is a constant proportionality between the r.m.s. and the hydrodynamic radius), this confirms the validity of Eq. (3). The retention of the sample follows the normal mode. In Fig. 2A the trend is the same but less conclusive because of the lower accuracy in the determination of the r.m.s. radius close to the size detection limit of the MALS detector and the high imprecision observed at the larger sizes.

### 4.2. Amylopectins

In order to investigate the effect of the flow-rates on the retention of amylopectins, first an estimation was made of the amount of amylopectins that can be injected without overloading the system. If too much of the analyte is injected, concentration effects of the analyte near the accumulation wall can distort the peak shape and create a shift in retention time [36]. To serve as an example for the amylopectins, the Lyckeby Stärkelsen amylopectin was fractionated with injected masses of between 0.2 and 5 μg. $F_{in}$, $F_{out}$ and $F_{cr}$ were 500, 390 and 110 μlmin$^{-1}$, respectively. In Fig. 3, the results are shown. With a sample load of between 0.2 and 0.5 μg the peak shape and retention time of the peak maximum remain unchanged. Evidently, overloading starts to take effect with injected masses larger than ca. 0.5 μg.

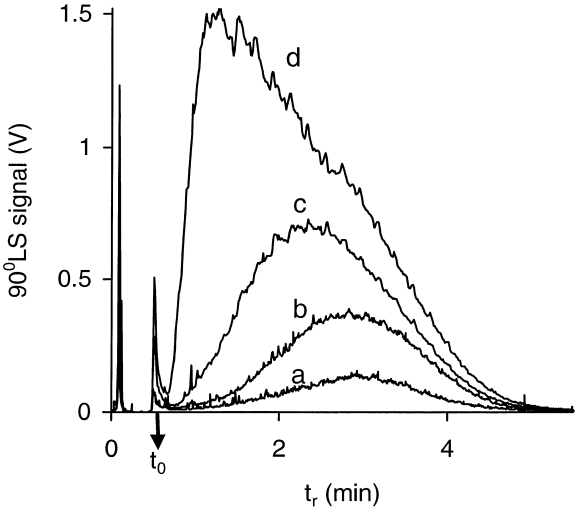


Fig. 3. Study of overloading. Superimposition of four fractograms of the Lyckeby Stärkelsen amylopectin. Set-up I. Injected masses: 0.2 (*a*), 0.5 (*b*), 2 (*c*) and 5 μg (*d*), respectively. $F_{in}$=500 μl min$^{-1}$. $F_{cr}$=110 μl min$^{-1}$; $t_0$=0.6 min.

To ensure the absence of overloading effects, an injected mass of 0.2 μg was preferred for a flow-rate study. However, such a small sample load is well below the detection limit of the RI detector and therefore only the MALS detector could be employed. Consequently, only the r.m.s. radius could be determined. All four amylopectin samples were subjected to similar flow conditions. The inlet flow was varied between 0.10 and 1.5 ml min$^{-1}$, while the ratio of $F_{out}$:$F_{cr}$ was kept constant at approximately 4:1.

In Fig. 4 two fractograms obtained of the Amioca amylopectin are shown. The amylopectins from the other three sources displayed similar trends. In Fig. 4A, at the lowest flow-rates ($F_{in}$, $F_{out}$ and $F_{cr}$ equal to 101, 80 and 21 μl/min, respectively) the amylopectin is retained but not size-fractionated, as the r.m.s. radius remains constant at approximately 450 nm over the main part of the peak. Rather than showing the size distribution in this range an average size is determined. Arguably, in the initial part of the peak the r.m.s. radius is observed to increase with

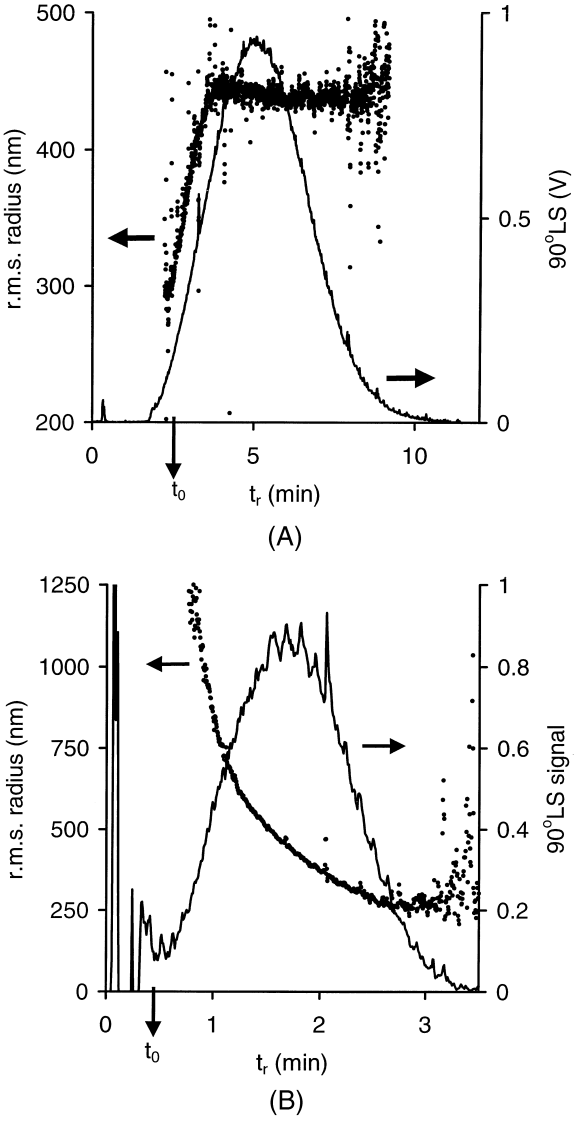


Fig. 4. Fractograms of Amioca at different flow-rates with determined r.m.s. radii. Set-up I. $F_{out}$:$F_{cr}$ were 80:21 (**A**) and 611:144 μl min$^{-1}$ (**B**). The calculated $t_0$ is indicated.

the retention time, which is an indication that the normal mode of elution might be operating here. When the inlet flow-rate was increased to $F_{in}$, $F_{out}$ and $F_{cr}$ of 755, 611 and 144 μl/min, respectively (Fig. 4B) the amylopectin is more retained and a size-fractionation is obtained. However, the order of elution of the components within the peak is opposite to that of the smaller degraded starches (Fig. 2).

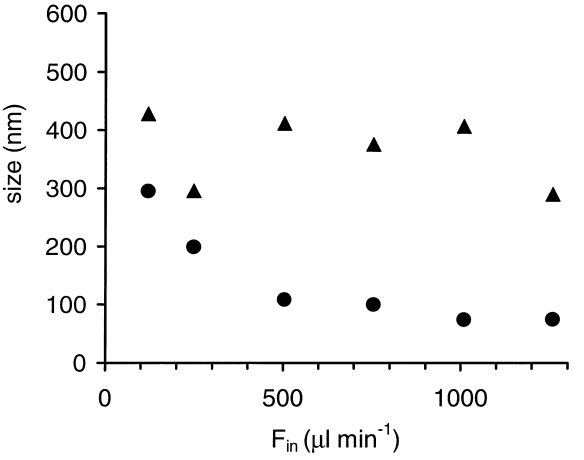


Fig. 5. Dependence of the apparent hydrodynamic radius (●) and r.m.s radius (▲), as measured at the peak maximum, on the inlet flow-rate with set-up I. Sample: Sigma amylopectin, injected mass 0.2 μg. Conditions: $F_{in}$, $F_{out}$ and $F_{cr}$ were 120, 100 and 21 μl min$^{-1}$; 247, 201 and 46 μl min$^{-1}$; 503, 408 and 95 μl min$^{-1}$; 755, 611 and 144 μl min$^{-1}$; 1009, 815 and 194 μl min$^{-1}$; 1258, 1008 and 250 μl min$^{-1}$, respectively.

One way of interpreting the type of results observed in Fig. 4B is to calculate the apparent hydrodynamic radius. Fig. 5 shows the apparent hydrodynamic radius at the peak maximum of the 90° MALS signal (calculated by Eq. (3)) as a function of the inlet flow-rates. Under ideal normal mode retention, the apparent hydrodynamic radius, is independent of the applied flow-rates [29]. In the present case, however, it strongly decreases with $F_{in}$. Also depicted in Fig. 5 is the r.m.s. radius at the same peak maximum and it can be seen that it, as expected, remains constant.

For a compact spherical molecule the r.m.s. radius is related to the hydrodynamic radius by the relationship $r_g = 0.775 \times r_H$ [22] whereas for a flexible polymer in a good solvent the relationship is $r_g = 1.862 \times r_H$. For amylopectin, being a highly branched polymer with presumably a globular structure, from multiangle static light scattering and dynamic light scattering a value of 1.3 has been found in the $r_g$ vs. $r_H$ relationship [37]. When this value is applied to the results in Fig. 5 it is obvious that for inlet flow-rates of larger than 0.5 ml min$^{-1}$ the apparent hydrodynamic radius is significantly smaller in relation to the r.m.s. radius than predicted. Although the determination of the r.m.s. radius is subject to an

uncertainty, it is clear that the apparent hydrodynamic radius is far from any true value for the hydrodynamic radius. In other words, the macromolecules show less retention than expected for the normal mode on basis of the r.m.s radius determined by MALS.

An explanation for the discrepant behaviour has to be found in one of the following possible deviations from normal mode behaviour in flow FFF: membrane interactions, viscosity effects, symmetry of the molecule, overloading or steric/hyperlayer effects. The observations are not likely to be caused by an experimental artefact. The calibration with ferritin and the results for pullulan and degraded starches show that the system is in good working order. In addition, the changes in elution order between Figs. 4A and 4B were obtained under identical conditions and processing of the MALS data with the exception of the flow-rates.

Overloading effects were ruled out previously (Fig. 2). Viscosity effects and interactions of the analyte with the membrane, are not likely to occur to a great extent as the peak shapes in Fig. 4 are smooth and not tailing. It has been argued that the orientation of highly asymmetrical, large macromolecules in a laminar flow can influence the diffusion coefficients that are obtained in flow FFF [22,38]. However, previous experiments have shown that amylopectins have a conformation between that of a spherical particle and a random coil [37], which rules out pronounced asymmetry as an explanation for the retention behaviour.

Multiple observations point towards the presence of steric/hyperlayer effects. First, the size fractionation in Fig. 4B is in reversed order. Moreover, it occurs at increased inlet flow-rates. Second, in Fig. 5 an increase in inlet flow leads to a lower $r_{H,app}$ (less retention). Lift forces are known to increase with an increased inlet flow-rate [39]. Steric/hyperlayer effects can also account for the lower hydrodynamic radius compared to the r.m.s. radius. The increased lift-force lifts the analyte further from the accumulation wall towards faster flow velocity lines, while the increasing cross-flow-rate insufficiently compensates this increase.

The results of Figs. 4B and 5 were further confirmed by a different set of experiments made on the Lyckeby Stärkelsen amylopectin after dissolution in water. Flow FFF analysis was made in water as the carrier liquid with an evaporative light scattering detector (ELSD) in set-up II. The only difference in the experiments compared to set-up I was that the channel had a 33% larger thickness. Fig. 6 shows examples of amylopectin peaks obtained at four different inlet flow-rates but at constant $F_{cr}$:$F_{out}$. The retention times were systematically decreasing at increasing inlet flow-rate and the calculated hydrodynamic radii were all much smaller than the predicted values. It was found that the amylopectin was eluted in much smaller time than expected from a calculation based on the hydrodynamic radius (200 nm) reported in literature [37]. This was in contrast to the behaviour of a dextran sample of the approximate molar mass $2\times10^6$ g mole$^{-1}$, which showed a retention time close to the predicted value. Actually, the amylopectin was eluted at retention times close to that of a much smaller dextran with a molar mass of $10\times10^3$ g mole$^{-1}$. These results are of the same character as those presented in Fig. 5 obtained with set-up I.

An estimation of the extent to which the lift forces work on the amylopectins can be made by examina-

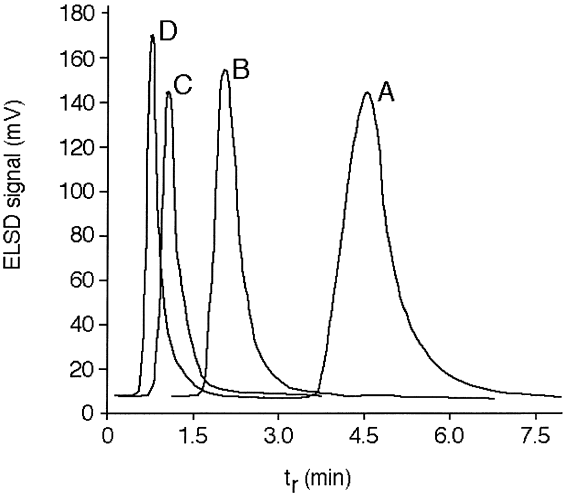


Fig. 6. Fractograms of the Lyckeby Stärkelsen amylopectin at constant $F_{cr}$:$F_{out}$=2.0 and varying $F_{in}$. Injected mass: 15 μg. Set-up II. A: $F_{in}$=1.0 ml min$^{-1}$, $F_{cr}$=0.7 ml min$^{-1}$, $F_{out}$=0.3 ml min$^{-1}$, $t_0$=0.69 min; B: $F_{in}$=1.5 ml min$^{-1}$, $F_{cr}$=1.0 ml min$^{-1}$, $F_{out}$=0.5 ml min$^{-1}$, $t_0$=0.45 min; C: $F_{in}$=2.0 ml min$^{-1}$, $F_{cr}$=1.2 ml min$^{-1}$, $F_{out}$=0.6 ml min$^{-1}$, $t_0$=0.38 min; D: $F_{in}$=3.0 ml min$^{-1}$, $F_{cr}$=2.0 ml min$^{-1}$, $F_{out}$=1.0 ml min$^{-1}$, $t_0$=0.23 min.

tion of the steric inversion radius. The steric inversion radius is defined as the radius above which steric inversion starts to take effect [26]. By definition, no material can be eluted beyond the steric inversion point. In Fig. 4B the graph of the r.m.s. radius decreases continuously in time until a value of ca. 290 nm at 2.5 min, after which the concentration comes close to zero and noise dominates the signal. This means that a steric and/or lift-hyperlayer mechanism is occurring for analytes with an r.m.s. radius from ca. 1 μm down to at least 290 nm, implying that the steric inversion radius must be 290 nm or smaller. The r.m.s. values at lower retention than the steric inversion point are obtained from a mixed-mode of material smaller than 290 nm in normal mode, and larger than 290 nm in steric/hyperlayer mode. Since 290 nm is at or near the steric inversion point the sample can be considered ''clean''–no mixed mode flow FFF occurs at the steric inversion point–and the r.m.s. value can be used for the calculation below. It is assumed in this approximation that amylopectin has a mono-modal size distribution.

There is however the rather unlikely possibility of a bimodal distribution of amylopectin, e.g., if we consider that a part of the amylopectin is 500 nm or larger, and another part is 100 nm or smaller (a gap in the distribution between 100 and 500 nm). It is then possible that the value of 290 nm doesn't reflect the steric inversion point (it could be at higher retention than the observed point), because there is no sample with the size of the steric inversion point. Then, the 290 nm is measured in a mixed-mode elution of 100 and 500 nm particles and therefore inaccurate.

An expression for the steric inversion radius ($r_i$) has been derived by Myers and Giddings [31]:

$$r_i = \sqrt{\frac{kT}{6\pi\eta\gamma u_{cr}}} \quad (6)$$

where $u_{cr}$ is the velocity of the cross-flow at the accumulation wall and $\gamma$ an empirical coefficient describing the extent to which hyperlayer effects are operative. When $\gamma$ is larger than unity micron-sized particles migrate faster than predicted by the steric mode. Hyperlayer effects can cause the faster migration. Here, $\gamma$ is assumed to be independent of the radius, which is not quite true. Combining this equation with $r_g = 1.3 \times r_H$ [37], $\gamma$-values of 6 to 8 were found for the Amioca amylopectin with inlet flows of between 0.75 and 1.25 ml $min^{-1}$ (for comparison, latex beads with a diameter of 15 μm and at an inlet flow-rate of 37.6 ml $min^{-1}$, showed a $\gamma$ value of almost 6 [40]). However, it should be noted that there are uncertainties in the determination of the r.m.s. radius and the ratio of $r_g/r_H$ (ratios of 1 to 1.3 were reported, depending on the treatment of the amylopectin) that have a strong effect on $\gamma$. Using a ratio of 1 leads to 40% smaller values for $\gamma$.

Nonetheless, the values of $\gamma$ found in our work, calculated on basis of the r.m.s. radius, are large at the low flow-rates employed. Apparently, the amylopectins behave as much larger molecules than can be expected on the basis of their size as measured by the r.m.s. radius. The hydrodynamic behaviour resembles that of a much larger molecule subject to significant hydrodynamic lift forces.

A more elaborate study of the effect of flow-rates on the retention of amylopectins may further clarify the observed behaviour. The key to this would be to choose conditions that minimise the magnitude of hydrodynamic lift-forces so that the retention behaviour comes closer to the normal mode. This may involve using both lower channel inlet/outlet flow velocities and possibly higher crossflow velocities, the latter counter-acting any lift-hyperlayer effects. The use of symmetrical flow FFF channels, in which channel and crossflow-rates can be chosen independently of each other, might be advantageous for such a study. In addition, a higher channel thickness may contribute to obtaining low channel inlet/outlet velocities.

### 4.3. Analysis of molar mass

A series of experiments was performed to analyse the molar mass of the amylopectins. The sample load was increased to 20 μg, the minimum amount required to obtain a reasonable RI signal. The fractionation was optimised in an empirical way. It was clear from previous experiments that a size fractionation is obtained at inlet flow-rates of 0.75 ml $min^{-1}$ and higher. An inlet flow-rate of 1.5 ml $min^{-1}$ was chosen. $F_{cr}$ was adjusted to 0.5 ml $min^{-1}$, so

that the analysis time for all samples remained smaller than ca. 5 min.

In Fig. 7 a typical fractogram is given of the National Starch amylopectin with the molar mass as obtained from the data. Due to peak overloading, as seen previously, there is no separation from the void peak. The maximum of the LS signal is at approximately the same retention time as that of the RI signal. Typically, in normal mode flow FFF of a polydisperse sample, the maximum of the MALS peak is at a larger retention time than that of the RI peak, because the sensitivity of the MALS detector increases with the molecular size, while the sensitivity of the RI detector is independent of it (see for example Fig. 2).

Fig. 7 reveals molar masses in the range of $10^7$ to $10^9$ g mol$^{-1}$. Due to the uncertainties in the calculations from the MALS signal, the given molar masses have to be regarded as approximate. Nonetheless, molar masses in this figure is of the same order of magnitude as those found by Bello-Pérez et al. using SEC-MALS [34] and larger than those measured by Fishman et al., who found for common maize (ca. 75% amylopectin) values of up to $3\times10^7$ g mol$^{-1}$ [6]. Besides the differences in origin of the sample the resulting molar mass can be highly dependent on the dissolution procedure for the amylopectin [11]. Bello-Pérez et al., applied a sophisticated microwave heating procedure after treatment of the amylopectin with DMSO, that enabled a more complete dissolution of the higher molar masses than in Fishman's work but at the risk of some de-polymerisation [34]. The sample preparation employed in our work is even milder. The stock solutions were clear and colourless. They can contain dissolved free molecules of amylopectin as well as aggregates [12]. To a certain extent the presence of aggregates can explain the observed hyperlayer phenomena as well as the large r.m.s. radii, although it cannot account for the small r.m.s. radius at which the inversion of elution order appears to take effect.

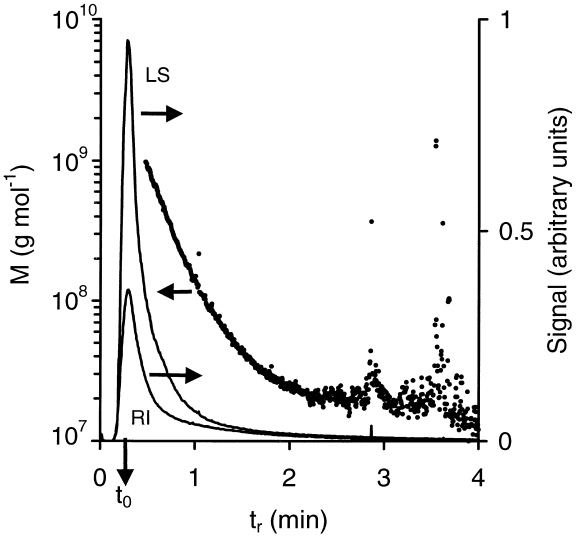


Fig. 7. RI and 90° LS fractograms of Amioca with apparent molar mass trace. Set-up I. The calculated $t_0$ is indicated. Conditions: see text.

## 5. Conclusions

It is clear from the presented results that the elution behaviour of amylopectins is strikingly different from that of degraded starches, which are of much smaller dimensions. While the degraded compounds show an increase of retention with size, the opposite is the case for amylopectins. Also, amylopectins display a strong dependence of the retention on the inlet flow-rate, and an apparent hydrodynamic radius far smaller than expected on basis of the determined r.m.s. radius. The most likely explanation for this behaviour is the occurrence of steric/hyperlayer effects. However, the r.m.s. radius at the steric inversion point is below the theoretically expected value, which may point towards an unexpectedly large hydrodynamic size for the amylopectin.

As in flow FFF the trend is towards the characterisation of ever larger macromolecules, in the years to come more investigation is required on the elution behaviour of very large polymers near the border of steric inversion. Possibly, a more elaborate study using channels of larger thickness and a greater variation of flow-rates can help elucidate the mechanism behind the observed behaviour.

## Acknowledgements

The financial support from the Swedish Research

Council for Engineering Sciences, the Swedish Natural Science Research Council, and the Swedish National Board for Industrial and Technical Development is acknowledged. Paul Mijland (AVEBE, Groningen, The Netherlands) is kindly acknowledged for his useful comments on the manuscript. This work was presented as a poster at the Eighth International Symposium on Field-Flow Fractionation, September 6–8 1999, Paris, France, and the 23rd International Symposium on Chromatography, 1–5 October 2000, London, UK.

## References

[1] J. Ellis, M.P. Cochrane, M.F.B. Dale, C.M. Duffus, A. Lynn, I.M. Morrison, R.D.M. Prentice, J.S. Swanston, S.A. Tiller, J. Sci. Food. Agr. 77 (1998) 289.
[2] J.D. Brewster, M.L. Fishman, J. Chromatogr. A 693 (1995) 382.
[3] J.A. Klavons, F.R. Dintzis, M.M. Millard, Cereal Chem. 74 (1997) 832.
[4] P.J. Wyatt, Anal. Chim. Acta 272 (1993) 1.
[5] J.Y. Chuang, in: C. Wu (Ed.), Handbook of Size Exclusion Chromatography, Marcel Dekker, New York, 1995.
[6] M.L. Fishman, L. Rodriguez, H.K. Chau, J. Agric. Food Chem. 44 (1996) 3182.
[7] S. You, S.-T. Lim, Cereal Chem. 77 (2000) 303.
[8] L.A. Bello-Perez, O. Parades-Lopez, P. Roger, P. Colonna, Cereal Chem. 73 (1996) 12.
[9] W. Yokoyama, J.J. Renner-Nantz, C.F. Schoemaker, Cereal Chem. 75 (1998) 530.
[10] M.M. Millard, F.R. Dintzis, J.L. Willett, J.A. Klavons, Cereal Chem. 74 (1997) 687.
[11] S. You, S.-T. Lim, Cereal Chem. 77 (2000) 303.
[12] Th. Aberle, W. Burchard, W. Vorberg, S. Radosta, Starch/Staerke 46 (1994) 329.
[13] M. Schimpf, K.D. Caldwell, J.C. Giddings (Eds.), Field-flow Fractionation Handbook, John Wiley and Sons, New York, 2000.
[14] J. Lou, M.N. Myers, J.C. Giddings, J. Liq. Chromatogr. 17 (1994) 3239.
[15] R. Hanselmann, M. Ehrat, H.M. Widmer, Starch/Staerke 46 (1995) 345.
[16] R. Hanselmann, W. Burchard, M. Ehrat, H.M. Widmer, Macromolecules 29 (1996) 3277.
[17] D. Roessner, W.-M. Kulicke, J. Chromatogr. A 687 (1994) 249.
[18] H. Thielking, D. Roessner, W.-M. Kulicke, Anal. Chem. 67 (1995) 3229.
[19] B.A. Korgel, J.H. van Zanten, H.G. Monbouquette, Biophys. J. 74 (1998) 3264.
[20] B. Wittgren, K.-G. Wahlund, J.Chromatogr. A 760 (1997) 205.
[21] B. Wittgren, K.-G. Wahlund, J. Chromatogr. A 791 (1997) 135.
[22] B. Wittgren, J. Borgström, L. Picullel, K.-G. Wahlund, Biopolymers 45 (1998) 85.
[23] C. Viebke, P.A. Williams, Food Hydrocolloids 14 (2000) 265.
[24] L. Picton, I. Bataille, G. Muller, Carbohyd. Polym. 42 (2000) 23.
[25] M.H. Cheng, P.J. Wyatt, Macromol. Symp. 140 (1999) 155.
[26] J.C. Giddings, Analyst 118 (1993) 1487.
[27] A. Litzén, K.-G. Wahlund, Anal. Chem. 63 (1991) 1001.
[28] A. Litzén, Anal. Chem. 65 (1993) 461.
[29] K.-G. Wahlund, J.C. Giddings, Anal. Chem. 59 (1987) 1332.
[30] B. Wittgren, K.-G. Wahlund, H. Dérand, B. Wesslén, Macromolecules 29 (1996) 268.
[31] M.N. Myers, J.C. Giddings, Anal. Chem. 54 (1982) 2284.
[32] J. Chmelík, J. Chromatogr. A 845 (1999) 285.
[33] M. Martin, J. Chromatogr. A 831 (1999) 73.
[34] L.A. Bello-Pérez, P. Roger, B. Baud, P. Colonna, J. Cereal Sci. 27 (1998) 267.
[35] B. Wittgren, M. Andersson, C. Arfvidsson, K.-G. Wahlund, J. Polym. Anal. Charact., in press.
[36] K.D. Caldwell, S.L. Brimhall, Y. Gao, J.C. Giddings, J. Appl. Polym. Sci. 36 (1988) 703.
[37] L.A. Bello-Pérez, P. Roger, P. Colonna, O. Paredes-López, Carbohyd. Polym. 37 (1998) 383.
[38] T. Pauck, H. Cölfen, Anal. Chem. 70 (1998) 3886.
[39] K.D. Caldwell, T.T. Nguyen, M.N. Myers, J.C. Giddings, Sep. Sci. Technol. 14 (1979) 935.
[40] J.C. Giddings, X. Chen, K.-G. Wahlund, M.N. Myers, Anal. Chem. 59 (1987) 1957.